Rare Metal Materials and Engineering
Volume 48, Issue 9, September 2019
Available online at www.rmme.ac.cn

Science Press

Cite this article as: Rare Metal Materials and Engineering, 2019, 48(9): 2729-2736.

ARTICLE

Formation and Expansion Behavior of Necklace Structure in Al-10Mg Alloy During Hot Uniaxial Compression

Mao Yizhe, Li Jianguo, Li Cong, Feng Lei

Key Laboratory of Advanced Materials of Ministry of Education, Tsinghua University, Beijing 100084, China

Abstract: The formation and expansion of necklace structure in an Al-10Mg alloy were studied. The alloy was produced by centrifugal casting, followed by 673 K/24 h solid solution treatment and hot uniaxial compression. The different effects of temperature and strain rate on expansion of necklace structure were particularly clarified. The results show that bulging is the nucleation type of first layer in necklace structure, and three different types of subboundary are found in the deformation microstructure. When the temperature increases, microband and recovered subboundary are gradually eliminated; strain-induced subboundary nucleation and recrystallized grain coarsening become the main way of necklace expansion. When the strain rate decreases, low angle grain boundary is accumulated. Three regions denoted by low misorientation region in interior, new grains in out layer and net structure of subboundary concentration in middle are observed in parent grains. The proportion of recrystallized grain area decreases when the strain rate changes from 6.94×10^{-1} s^{-1} to 6.94×10^{-2} s^{-1}, and then significantly increases as strain rate further decreases from 6.94×10^{-2} s^{-1} to 6.94×10^{-3} s^{-1}.

Key words: Al-10Mg alloy; uniaxial compression; dynamic recrystallization; necklace structure; formation and expansion

Al-Mg alloy plays an important role in offshore manufacturing, transportation and aerospace industries for its high strength-to-weight ratio, high corrosion resistance and good welding performance. Microbands in Al-Mg alloys deformed at room temperature are analogous to that in cell forming metals[1-4]. Microband is a dislocation substructure including long straight dislocation boundaries that are nearly parallel to {111} slip planes[5, 6]. To achieve higher strength for better application, increasing Mg content is an effective way of solid solution strengthening with 13% diameter deviation between Mg and Al atoms. However, solute effect increases the friction stress, causing cracks in early strain, especially in severe deformation[7-10], which needs to increase deformation temperature.

An empirical formula was proposed to describe the parameter of dynamic recrystallization (DRX) occurring in hot deformation[11], which is as follows:

$$\ln Z \leq (1/b)\ [1/D_0(-\varepsilon)^{-a}] \qquad (1)$$

where Z is a parameter related to strain rate, temperature and deformation activity energy Q, D_0 is the initial grain size, ε is the deformation strain, and a and b are constants. Traditionally, DRX is divided into two thermodynamic processes: nucleation with high angle grain boundary (HAGB) formation, and new grain coarsening with HAGB migration. Generally, there are two types of DRX. The first is continuous dynamic recrystallization (CDRX)[12-15], during which subgrain forms by dislocation recovery in interior of parent grain. The second is discontinuous dynamic recrystallization (DDRX)[16, 17], during which necklace new grain structure forms for the bulging of prior grain boundaries (GBs) followed by necklace structure expansion. But only geometric dynamic recrystallization (GDRX) was observed in pure aluminum and low magnesium Al-Mg alloys[18]. DDRX was found in Al-6Mg alloys, while CDRX was found in Al-Mg-Mn-Sc-Zr alloys[19-28]. For higher Mg level, more details, especially the different effects of temperature and strain rate on DRX, are still unclear.

In the present work, solid solution treated Al-10Mg alloy was subjected to uniaxial compression at different tempera-

---

Received date: September 09, 2018
Foundation item: International Science & Technology Cooperation Program of China (2015DFR50470)
Corresponding author: Li Jianguo, Ph. D., Associate Professor, School of Material Science and Engineering, Tsinghua University, Beijing 100084, P. R. China, Tel: 0086-10-62791092, E-mail: jg.li@mail.tsinghua.edu.cn

tures and strain rates. The flow stress behavior was tested by Gleeble 1500, and the microstructure evolution, especially the formation and expansion of the necklace structure, was characterized by electron backscattered diffraction (EBSD).

1 Experiment

For its high Mg content, Al-10Mg binary alloy was selected in this study. Commercially pure aluminum and pure magnesium were melted in a medium-frequency induction furnace, and 0.2 wt% Al-5Ti-1B was added for grain refinement. Then, the metallic fluid was cast in a vertical centrifugal casting machine that rotates at G=100, where G is the gravity in centrifuge field. To eliminate magnesium segregation, casting ingots were homogenized at 673 K for 24 h before plastic deformation. Composition of the Al-10Mg alloy is listed in Table 1.

Φ8 mm×12 mm cylindrical specimens were machined from ingots. Uniaxial compression test was carried out on Gleeble 1500 with true strain of ε=−1.1 at 573, 623 and 673 K, under strain rate of 6.94×10^{-3}, 6.94×10^{-2} and 6.94×10^{-1} s^{-1}. Graphite paper was placed on both sides of indenter end plane to eliminate the friction effect. Immediate water quenching was performed after compression. Each test was performed three times for the accuracy of results. Longitudinal section of compressed specimen was electrochemically polished, and the corresponding specimen coordinate system is schematically shown in Fig.1. The microstructure was characterized by EBSD with accelerating voltages of 15 and 20 kV and a scan step size of 0.06~0.3 μm.

2 Results and Discussion

2.1 Flow stress behavior of Al-10Mg alloy

The sensitivity of stress to temperature and strain rate is shown in Fig.2a~2c. Compressive stress decreases with increasing the temperature. Notable softening effect after peak stress is found when compressed at 623 and 673 K, while curve has a steady stage after rapid growth without stress drop when compressed at 573 K and 6.94×10^{-1} s^{-1}. Al-10Mg alloy is sensitive to strain rate, and a positive correlation between stress and strain rate was found. In addition, notable stress drop in stress-strain curve occurs only at 6.94×10^{-3} s^{-1}. On the one hand, critical stress of dislocation slipping decreases with increasing the temperature, because the amplitude of atomic thermal vibration increases[29-31]. On the other hand, the multiplication and entanglement of dislocation are intensified when deformation strain rate increases.

Table 1 Chemical composition of Al-10Mg alloy (wt%)

Mg	Fe	Si	Al
9.67	0.094	0.058	Bal.

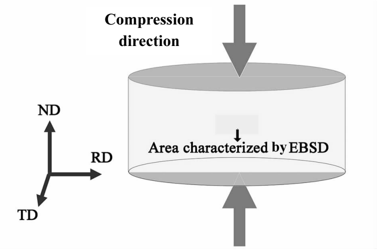

Fig.1 Compression direction, specimen coordinate system, and area characterized by EBSD

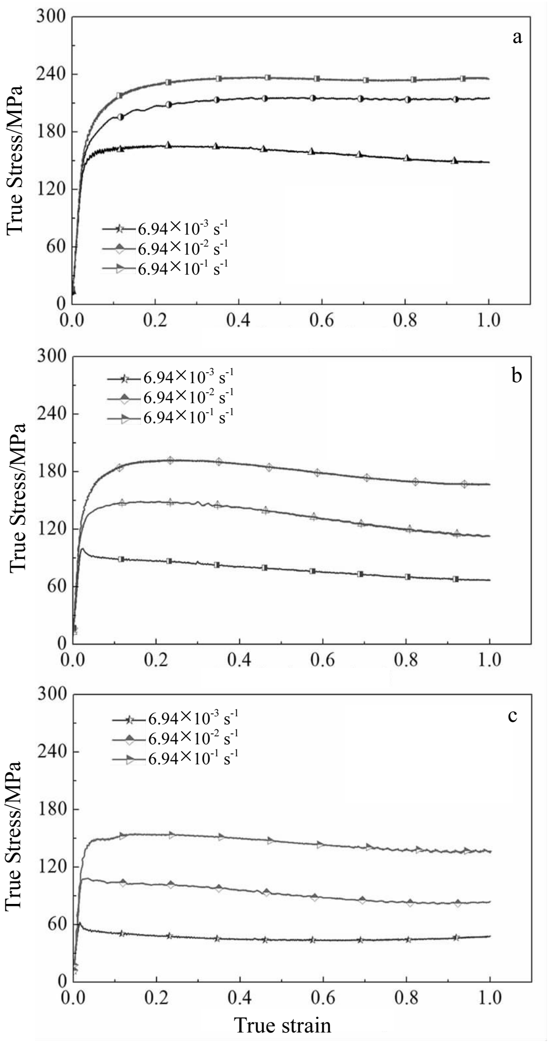

Fig.2 True stress-true strain curves of Al-10Mg alloy at 573 K (a), 623 K (b) and 673 K (c) under different strain rates

Stress-strain curve is a macroscopic competition performance between work hardening and dynamic recovery as well as recrystallization softening. The different influences of temperature and strain rate need to be further studied by further microstructure characterization.

2.2 Necklace structure formation behavior in Al-10Mg alloy

Inverse pole figure (IPF) of specimen compressed at 573 K and 6.94×10^{-1} s^{-1} is shown in Fig.3a. Misorientation profiles parallel and vertical to microband in a violent grain were calculated. Point-to-point misorientation along L1 is less than 1.5° (Fig.3b), and accumulative misorientation is up to 14°. Microbands' angle along L2 was in the range of 2°~5°. However, grains with bigger Schmid factor have almost no microband. These grains are oriented favorably to accommodate strains, and thus can undergo larger deformation without subdivision.

Although there is no obvious stress drop in stress-strain curve, dynamic recrystallized grains do exist at GBs (hereinafter referred to "boundary grains") and microband (referred as "microband grains"). Only single or double layers of necklace structure exist. Three rows of "microband grains" in a blue parent grain (labeled by dash frame) were observed.

Magnified IPF maps are shown in Fig.4 to reveal the DRX behavior occurring in Al-10Mg compressed at 573 K and 6.94×10^{-1} s^{-1}. Bulging nucleation mechanism[32,33] that causes the formation of first layer of necklace structure[34] was observed, as shown in Fig.4a. Serrated boundary between two parent grains traverses the whole figure, and there are six new grains numbered 1 to 6 sequentially on it. Subgrains 2 and 3 have the same color with parent grains. Grains 1, 4, 5, and 6 are new grains with a full set of HAGB. Miura et al[32] found that grain boundary shearing, which takes place in early stage, leads to serrated boundaries and inhomogeneous local strain gradients. Serrated boundary then turned into bulging when strain increased, and inhomogeneous local strain gradients were added up to LAGB at bulging shoulders. It is called "strain-induced subboundary"[35]. Then, subgrain would form as if it was cut off from parent grains, such as subgrains 2 and 3. LAGBs caused by dynamic recovery would also interact with strain-induced subboundary, and assist forming subgrains. With the increase of strain, grain rotation would produce bigger misorientation, and subboundaries turn into HAGBs. Then, the first layer of necklace structure is formed.

After the formation of first layer, the necklace structure expansion was analyzed (Fig.4b). The new grains of the first layer are embedded in parent grains, which surges the bulging of parent grain boundaries. Compared with the formation of the first layer, the necklace structure expansion is much easier because of the severer bugling. Strain-induced subboundaries at embedded tips are marked with several red arrows. Misorientation profile along L3 that crosses two strain-induced subboundaries was calculated (Fig.4d). One angle peak is 7.5°, and the other is 3.5°. Two adjacent strain-induced subboundaries are linked together to form a new subgrain, and this is the ordinary method for necklace structure expansion. Sometimes long strain-induced subboundary linked with microband produces subgrain in unstable shape. The initial stage of abnormal subgrain is marked with black dashed frame (Fig.4b), and several strain-induced subboundaries form in it. The reason for abnormal subgrain division is that hexagon shape and interfacial tension equilibrium condition are not satisfied. There is a transition stage before reaching the final DRX structure. It is called "subgrain fission mechanism" in this paper.

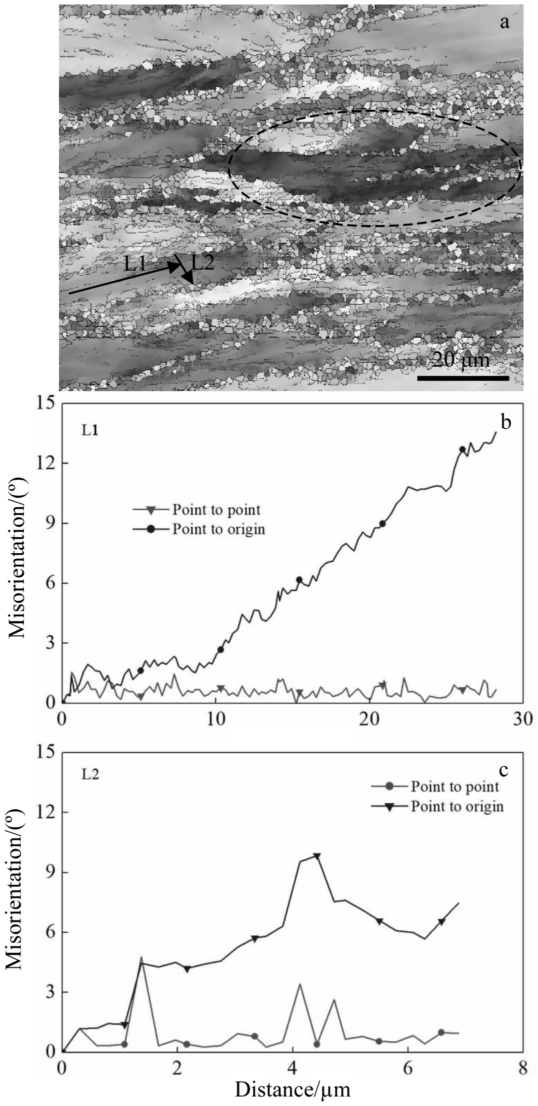

Fig.3 IPF map at 573 K and 6.94×10^{-1} s^{-1} (a); misorientation profiles measured along L1 (b) and L2 (c)

Four deformation bands and three layers of "microband grains" are marked in Fig.4c. Layers fenced by dashed lines are the initial stage of DRX, in which bulging boundaries in subgrains were observed. There are two types of microband in Al-Mg alloy[1]. At early stage, single dislocation boundary, called domain boundary, formed. When strain increased, more complex dislocation boundaries composed of several DBs formed, called microband. Plate-like regions formed inside the microband, which are front status for nucleation of "microband grains". Region fenced by red wireframe shows the expansion of "microband grains". HAGBs and LAGBs formed in deformation band 3 on the right side. The orientation of those boundaries is nearly perpendicular to layers' tangents. It is known that a grain would be divided into several strip regions, called deformation band, by microbands, in which

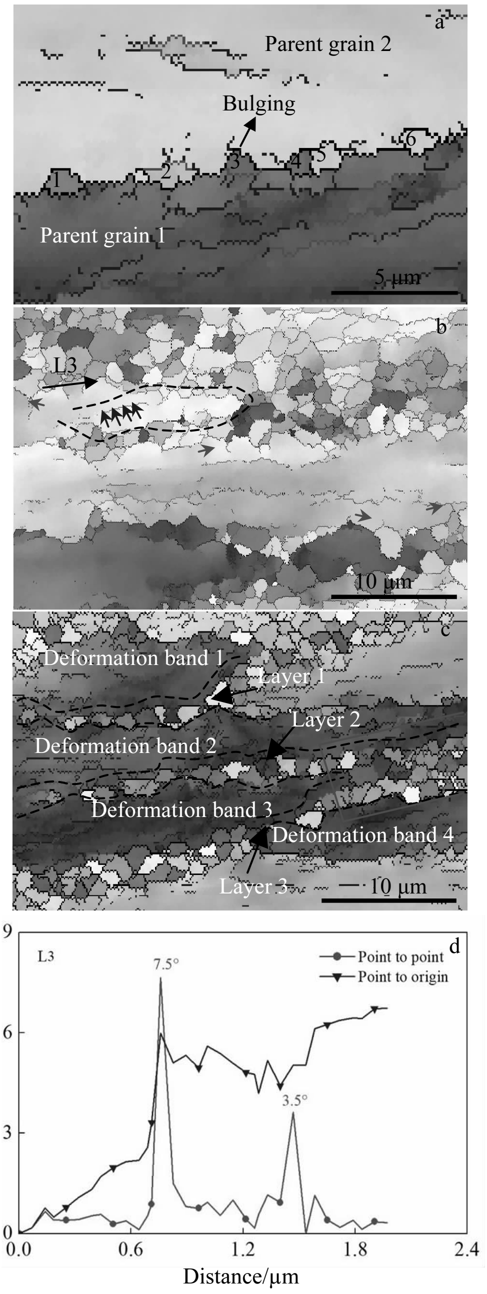

Fig.4 Bulging nucleation magnified map (a); first layer of necklace structure expansion (b); grain's nucleation and expansion (c); misorientation profiles measured along L3 in Fig.4b (d)

strain-induced subboundary formed inside. Dislocation slip and cross slip occurred to minimize subboundaries' length. Then, subgrain formed, causing "microband grain" expansion.

2.3 Expansion behavior when temperature increases

Fig.5 shows IPF maps of specimen compressed at 623 and 673 K at 6.94×10^{-1} s^{-1}. Parent grains still exist, but no microband is found (Fig.5c and 5d). Two types of LAGB exist inside the parent grains, some of them are linked with HAGBs, while others randomly float inside. The former is strain-induced subboundaries, and the latter are originated due to dislocation recovery. At high temperature, dynamic recovery is mainly controlled by dislocation climb, which results in floating subboundary emission.

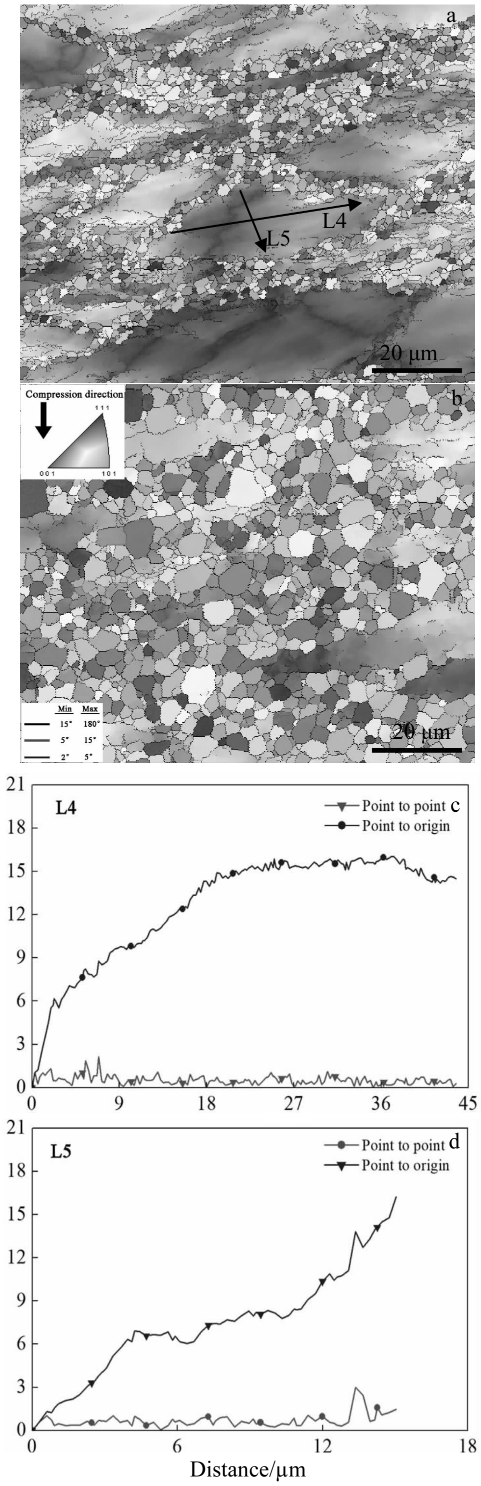

Fig.5 IPF maps of specimen compressed at 623 K (a) and 673 K (b) under 6.94×10^{-1} s^{-1}; misorientation profiles measured along L4 (c) and L5 (d)

New grains apparently grew when temperature increased

(Fig.5b). Bulging of HAGB and plate-like region in microband are two types of nucleation. The interaction of strain-induced subboundary and microband is the main way for necklace structure expansion. However, with increasing the temperature, the percentage of LAGBs mentioned above gradually decreases (Fig.6). The effect of new grain coarsening on expansion becomes more important. Increasing temperature can make it much easier for grain boundary migration.

A size genetic effect when temperature increases is proposed, as schematically shown in Fig.7a. It assumes that three new grains are stable in standard hexagon shape, and *a* is the side-length of hexagonal new grain. Parent grain boundary adjacent to them is serrated by shearing stress. Strain-induced subboundaries are produced at tips of interface, causing the development of subgrain whose size has a positive correlation with *a*. Therefore, the size of subgrain increases when temperature increases, and the size of new grains increases.

Subgrain fission mechanism mentioned above was also observed when temperature increased. The initial stage and ideal latter stage are shown in Fig.7b~7d. Double parallel strain-induced subboundaries exist (Fig.7b), and two end points of them inside the parent grain are linked together by recovered subboundary. Subgrain formed with irregular polygons shape. Then the second generation of strain-induced subboundary was produced by adjacent new grain (Fig.7c). Fig.7d shows the ideal fission mechanism among new grains. Unstable new grain, especially in concave polygon shape, would be divided into several subgrains. To some extent, subgrain fission mechanism leads to further grain refinement during DRX, which would be effective against grain coarsening. It is assumed that the number of new grains remains unchanged and abnormal grain growth is not considered. The tendency of new grain size is schematically shown in Fig.8. T_i (i=1, 2, 3) is the deformation temperature, and "a_i" is the equivalent side-length of hexagon. For subgrain fission mechanism, dynamic recrystallized grain size becomes much more concentrated with lower standard deviation.

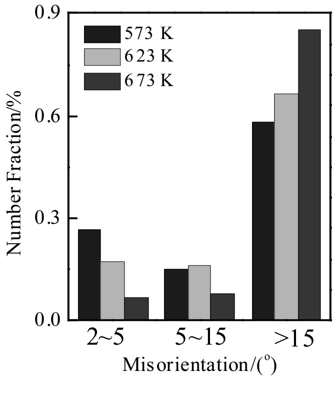

Fig.6 Number fraction of LAGBs and HAGBs as temperature increases

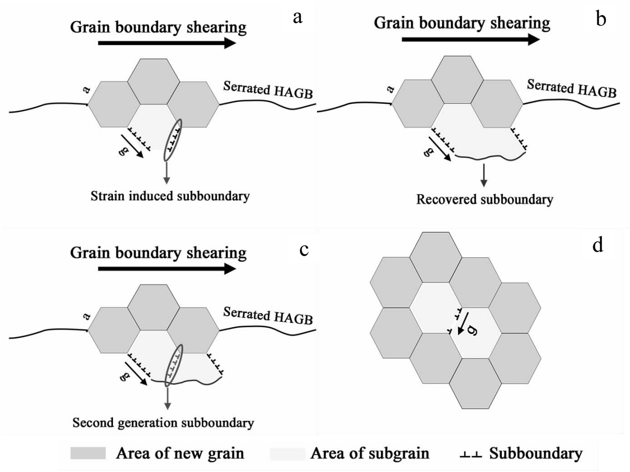

Fig.7 Size genetic effect (a); formation of irregular subgrain (b); subboundary of the second generation of strain-induced subboundary (c); ideal fission mechanism among new grains (d)

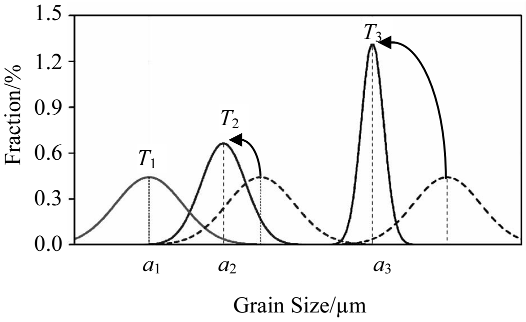

Fig.8 Change of new grain size when temperature increases under several assumptions

2.4 Expansion behavior when strain rate decreases

Fig.9 shows IPF maps of specimen compressed at 6.94×10^{-2} s^{-1} and 6.94×10^{-3} s^{-1} at 573 K. Misorientation profiles in a violent grain along L6 and L7 in Fig.9a were calculated, and no microband was observed. New grain area fraction decreases compared with that at higher strain rate. It is because enough time is given for dislocation cross slipping, and strain spreads more uniformly. When strain rate decreases, there is no enough activation energy for more DRX. However, sensible increase of new grain area fraction occurred when strain rate dropped to 6.94×10^{-3} s^{-1}. The number fraction of LAGBs and HAGBs with decreasing the strain rate is shown in Fig.10. The fraction of HAGBs decreases when strain rate decreases from 6.94×10^{-1} s^{-1} to 6.94×10^{-2} s^{-1}, and then increases when strain rate decreases to 6.94×10^{-3} s^{-1}. Region 2 and region 3 are two parent grains, which were separated into three areas: low misorientation in center, new grains in outer layer, and subboundaries concentration in medium area. Misorientation profiles of region 3 are listed in Fig.9f and 9g. Floating HAGBs in region 2 was caused by dislocation recovery, which was linked with strain-induced subboundaries and other recovered sub-

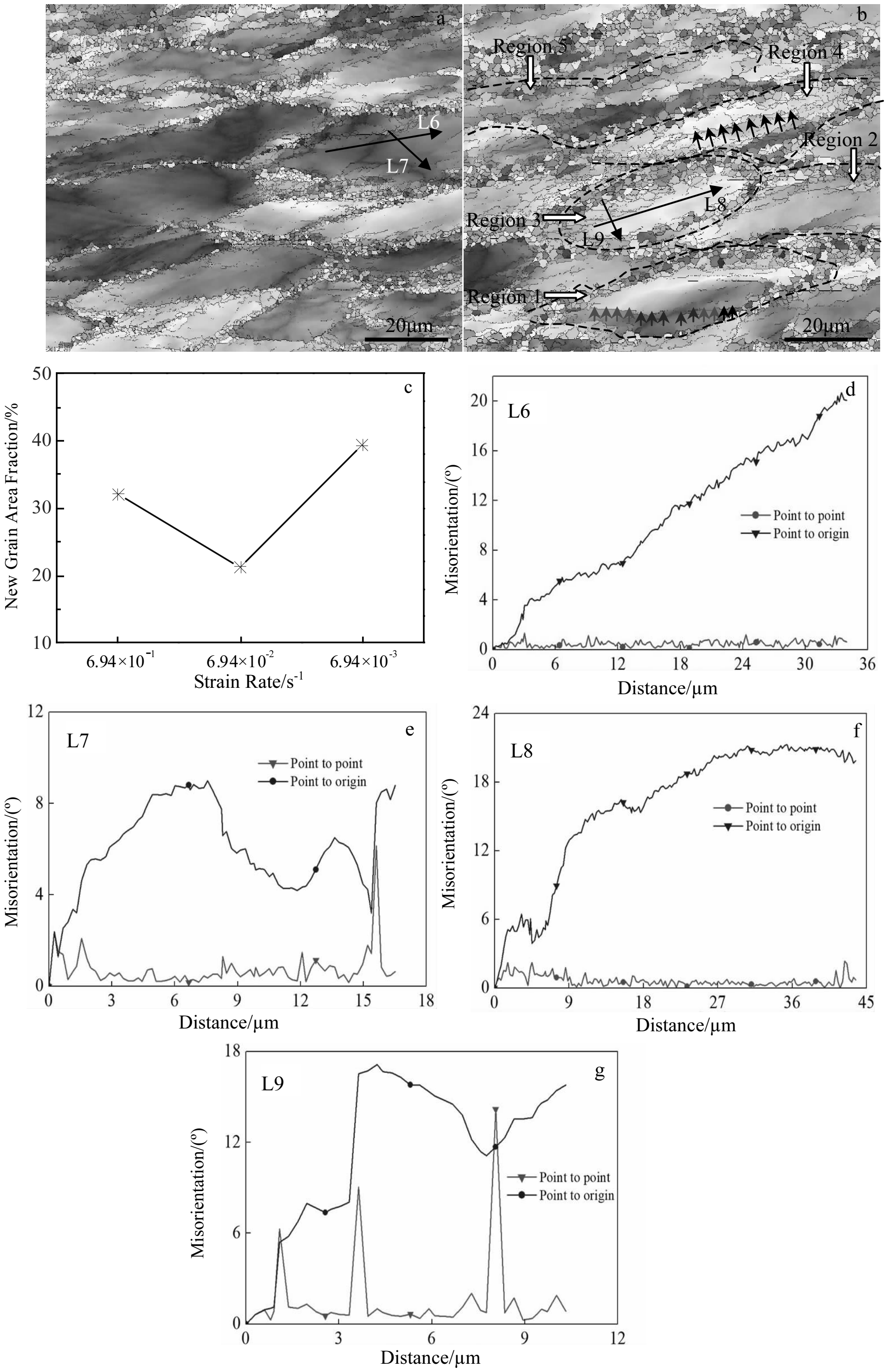

Fig.9 IPF maps at 6.94×10^{-2} s^{-1} (a) and 6.94×10^{-3} s^{-1} (b) at 573 K; (c) plot of new grain area fraction at 573 K; (d~g) misorientation profiles measured along L6~L9

boundary segments, causing a net structure of subboundaries. Subgrain is the prior state of new grain formation, so there is a sensible increase in new grain area fraction at 6.94×10^{-3} s^{-1}. Regions 4 and 5 are grains with long single walls in the middle. Wall in region 4 is marked with a row of black arrows, and net structure forms on both sides of walls. Region 1 contains the initial stage of long single wall formation. Long strain-induced subboundaries spread into grain, and recovered subboundaries are linked with them, which are marked with a row of colored arrows. In this row of colored arrows, red one corresponds to LAGB in the range of 5°~15°, blue corresponds to 2°~5°, and black corresponds to HAGB.

The above discussion in this section is schematically shown in Fig.11. Fig.11a contains the "three area division", and Fig.11b contains the "long single wall". As shown in Fig.9b, decreasing strain rate accelerates the spread of strain-induced subboundary in longitudinal orientation. At high strain rate, dynamic recovery and DRX compete for active energy. However, at low strain rate, dynamic recovery becomes the initial stage of recrystallization, providing subgrain nucleation in the interior of parent grain, which mainly transforms into CDRX.

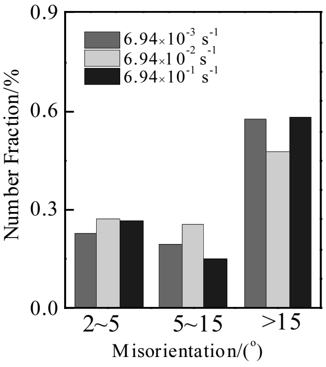

Fig.10 Number fraction of LAGBs and HAGBs as strain rate decreases

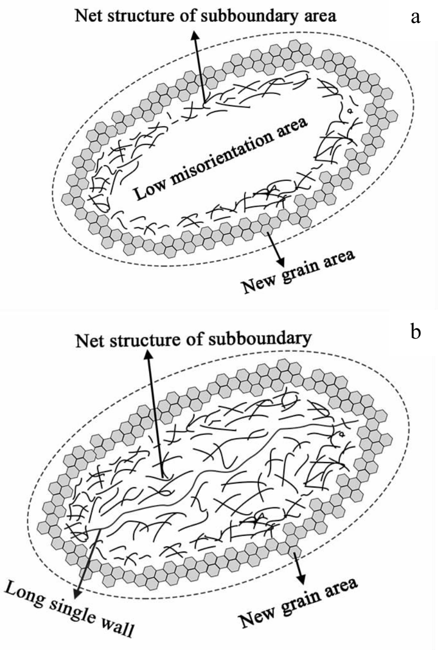

Fig.11 Three region division (a) and long single wall (b)

3 Conclusions

1) Microband can be observed in specimen compressed at 573 K at 6.94×10^{-1} s^{-1}. The first layer of necklace structure forms through bulging mechanism.

2) When temperature increases, low angle grain boundary gradually disappears. Necklace structure expansion is mainly caused by high angle grain boundary migration.

3) The proportion of recrystallized grain area decreases when strain rate changes from 6.94×10^{-1} s^{-1} to 6.94×10^{-2} s^{-1}, subboundary is accumulated, and then improved when strain rate changes from 6.94×10^{-2} s^{-1} to 6.94×10^{-3} s^{-1}. The accumulated low angle grain boundary gradually turns into high angle grain boundary.

References

1 Hughes D A. *Acta Metallurgica et Materialia*[J], 1993, 41(5): 1421

2 Bay B, Hansen N, Hughes D A. *Acta Metallurgica et Materialia*[J],1992, 40(2): 205

3 Kuhlmann-Wilsdorf D. *Materials Science and Engineering A*[J], 1989, 113(1): 1

4 Kuhlmann-Wilsdorf D, Comins N R. *Materials Science and Engineering*[J],1983, 60(1): 7

5 Driver J H, Papazian J M. *Materials Science and Engineering*[J], 1985, 76: 51

6 Nakayama Y, Morii K. *Acta Metallurgica*[J], 1987, 35(7): 1747

7 Zha M, Li Y J, Mathiesen R H *et al*. *Materials Science and Engineering A*[J], 2014, 598(26): 141

8 Liua X Y, Adamsb J B. *Acta Materialia*[J], 1998, 46(10): 3467

9 Song R G, Tseng M K, Zhang B J *et al*. *Acta Materialia*[J], 1996, 44(8): 3241

10 Valds-Tabernero M A, Sancho-Cadenas R, Sabirov I *et al*. *Materials Science and Engineering A*[J], 2017, 696(1): 348

11 Chang Hai, Wang Xiaojun, Hu Xiaoshi *et al*. *Rare Metal Materials and Engineering*[J], 2014, 43(8): 1821

12 McQueen H J. *Philosophical Magazine A*[J], 1989, 60: 447

13 Gourdet S, Montheillet F. *Materials Science and Engineering A*[J], 2000, 283(1-2): 274

14 Musin F, Belyakov A, Kaibyshev R *et al*. *Reviews on Advanced Materials Science*[J], 2010, 25: 107

15 Giovanni Maizza, Renato Pero, Maria Richetta *et al*. *Journal of Materials Science*[J], 2018, 53(6): 4563

16 Doherty R D, Hughes D A, Humphreys F J *et al*. *Materials Science and Engineering A*[J], 1997, 238(2): 219

17 Lin Y J, Liu W C, Wang M *et al*. *Materials Science and Engineering A*[J], 2013, 573(20): 197

18 Henshall G A, Kassner M E, Mcqueen H J. *Metallurgical Transactions A*[J], 1992, 23(3): 881

19 Nieh T G, Hsiung L M, Wadsworth J *et al*. *Acta Materialia*[J], 1998, 46(8): 2789

20 Peng Haijian, Li Defu, Guo Qingmiao *et al*. *Rare Metal Materials and Engineering*[J], 2012, 41(8): 1317

21 He Yongdong, Zhang Xinming. *Rare Metal Materials and Engineering*[J], 2009, 38(11): 1945

22 Yan J, Pan Q L, Zhang X K *et al*. *Journal of Central South Uni-*

versity[J], 2017, 24(3): 515

23 Chen Q, Pan Q L, Peng H *et al*. *The Chinese Journal of Nonferrous Metals*[J], 2012, 22(6): 1555

24 Zhang Y H, Yin Z M, Zhang J *et al*. *Rare Metal Materials and Engineering*[J], 2002, 31(3): 167

25 Pan Q L, Yin Z M, Zou J X *et al*. *Materials Science and Technology*[J], 2001, 7: 749

26 Feng Di, Zhang Xinming, Liu Shengdan *et al*. *Rare Metal Materials and Engineering*[J], 2016. 45(8): 2104 (in Chinese)

27 Zhou Wei, Ge Peng, Zhao Yongqing *et al*. *Rare Metal Materials and Engineering*[J], 2012, 41(8): 1381 (in Chinese)

28 Liu Yi, Xu Kun, Luo Xinming *et al*. *Rare Metal Materials and Engineering*[J], 2013, 42(9): 1820 (in Chinese)

29 Fan G J, Wang G Y, Choo H *et al*. *Scripta Materialia*[J], 2005, 52(9): 929

30 Bernard C, Coer J, Laurent H *et al*. *Experimental Mechanics*[J], 2017, 57(3): 405

31 Jobba M, Mishra R K, Niewczas M. *International Journal of Plasticity*[J], 2015, 65: 43

32 Miura H, Aoyama H, Sakai T. *Journal of the Japan Institute of Metals*[J], 1994, 58(3): 267

33 Sakai T, Belyakov A, Kaibyshev R *et al*. *Progress in Materials Science*[J], 2014, 60: 130

34 Pong D, Gottstein G. *Acta Materialia*[J], 1998, 46(1): 69

35 Ji F Q. *Advanced Materials Research*[J], 2014, 887-888: 395

Al-10Mg 合金热压缩过程中项链组织的形成和扩展行为

毛轶哲，李建国，李 聪，封 蕾

(清华大学 先进材料教育部重点实验室，北京 100084)

摘 要：采用旋转结晶工艺制备高镁含量的 Al-10Mg 合金坯料，并对其进行 673 K/24 h 固溶处理及单轴热压缩变形。通过流变应力行为及微观组织表征来分析合金动态再结晶过程中项链组织的形核及扩展行为，特别地，分析了变形温度和应变率对项链组织扩展行为的不同影响。研究表明：大角度晶界的凸出是项链组织首层再结晶晶粒的形核方式, Al-10Mg 合金变形组织中有微带、应变诱发的小角度晶界和回复形成的小角度晶界等 3 种亚晶界。随变形温度升高，微带和回复形成的小角度晶界逐渐消失，应变诱发的小角度晶界形核及由大角度晶界迁移造成的再结晶晶粒粗化是项链组织扩展的主要方式；随应变率的降低，未再结晶的变形晶粒被划分为低取向差中心区、外层再结晶晶粒区和处于中间层的富集小角度晶界的网状结构区等 3 部分，应变率从 6.94×10^{-1} s^{-1} 降至 6.94×10^{-2} s^{-1} 时再结晶晶粒面积占比减小，而当应变率从 6.94×10^{-2} s^{-1} 进一步降至 6.94×10^{-3} s^{-1} 时，再结晶晶粒面积占比显著提高。

关键词：Al-10Mg合金；热压缩；动态再结晶；项链组织；形核及扩展

作者简介：毛轶哲，女，1992 年生，硕士，清华大学材料学院先进材料教育部重点实验室，北京 100084，电话：010-62791092，E-mail: maoyizhebit@126.com